

## Electron momentum distribution in graphite and lithium-intercalated graphite

M. Y. Chou, Steven G. Louie, and Marvin L. Cohen

*Department of Physics, University of California,  
and Materials and Molecular Research Division,  
Lawrence Berkeley Laboratory, Berkeley, California 94720*

N. A. W. Holzwarth

*Department of Physics, Wake Forest University,  
Winston-Salem, North Carolina 27109*

(Received 20 March 1984)

Compton profiles of the first-stage graphite intercalation compound  $\text{LiC}_6$  have been calculated using the self-consistent pseudopotential method within the local-density-functional formalism. The difference between profiles of  $\text{LiC}_6$  and graphite exhibits characteristic features which provide further elucidation of the electronic properties of intercalation. It is found that the change in the electron momentum distribution in  $\text{LiC}_6$  is qualitatively different from that predicted by the generally accepted rigid-band model.

Graphite is a prototype material for the investigation of two-dimensional solids. In addition its properties can be changed dramatically by diffusing atoms or molecules into the interlayer spaces,<sup>1,2</sup> yielding physically interesting materials with potentially important technological applications. Recently, the electronic properties of the first-stage lithium-intercalated graphite  $\text{LiC}_6$  have been studied intensively experimentally.<sup>3-6</sup> The motivation of this work is to use theoretical methods to explore both qualitatively and quantitatively how the graphite energy levels change with the introduction of lithium atoms, and the role of the lithium  $2s$  electron.

Detailed self-consistent band-structure calculations for graphite<sup>7</sup> and  $\text{LiC}_6$ ,<sup>8</sup> have been performed using the pseudopotential method<sup>9</sup> within the local-density-functional scheme.<sup>10,11</sup> Here, we examine the properties of the electrons in momentum space. This provides a new point of view in interpreting the electronic structure. The momentum distributions (Compton profiles) of the valence electrons for both graphite and  $\text{LiC}_6$  are calculated using the wave functions obtained from previous self-consistent calculations.<sup>7,8</sup> The calculated anisotropy for the Compton profiles of graphite is in excellent agreement with observations. The predicted difference between profiles of  $\text{LiC}_6$  and graphite show some special characteristics which should be tested in further experimental studies of the electronic properties of  $\text{LiC}_6$ . In particular, the commonly used rigid-band

model yields a qualitatively different result for the Compton-profile differences.

The band-structure calculations are done using the exchange-correlation potential of Hedin and Lundqvist<sup>12</sup> and norm-conserving pseudopotentials.<sup>13</sup> The wave functions in the crystal are represented by a mixed basis set consisting of plane waves and linear combinations of atomic orbitals.<sup>14</sup> For graphite, the results for the occupied bands are consistent with other calculations,<sup>15</sup> and with results of an angle-resolved photoemission experiment.<sup>4</sup> For  $\text{LiC}_6$ , the intercalation of lithium causes a 10% expansion in the interlayer separation and changes the layer stacking pattern from  $ABAB$  in graphite to  $A\alpha A\alpha$ .<sup>16</sup> The occupied energy bands of  $\text{LiC}_6$  look very similar to those of graphite folded into the new Brillouin zone except for some small nonuniform shifts. The extra valence electron (donated by lithium) fills part of the  $\pi$  antibonding orbitals which are only slightly occupied in graphite. This results in an increased Fermi level, as is predicted by the rigid-band model.

Using the calculated wave functions, the projected momentum distribution of the valence electrons along specific directions is computed. These can be measured experimentally in the Compton profiles via electron-photon scattering process. If the wave functions are expanded in plane waves, within the impulse approximation<sup>17</sup> the expression for the Compton profile along a specific direction  $\hat{e}$  is

$$J(q, \hat{e}) = \frac{1}{N} \sum_n \sum_{\vec{k}} \sum_{\vec{G}} |C_{n, \vec{k}}(\vec{G})|^2 \theta(E_F - E_{n, \vec{k}}) \delta[(\vec{k} + \vec{G}) \cdot \hat{e} - q], \quad (1)$$

where  $C_{n, \vec{k}}(\vec{G})$  is the coefficient of the plane-wave component  $e^{i(\vec{k} + \vec{G}) \cdot \vec{r}}$  for the state  $\Psi_{n, \vec{k}}(\vec{G})$  with energy  $E_{n, \vec{k}}$ ,  $n$  represents the band index, and  $E_F$  is the Fermi energy. About 600 and 900 reciprocal lattice vectors,  $G$ 's, are included for graphite and  $\text{LiC}_6$ , respectively. The tetrahedron linear interpolation method<sup>18</sup> is employed in performing the summation over the  $k$  points in the Brillouin zone, and a grid of 45  $k$  points in the irreducible zone is used. Figure 1 shows the calculated valence electron profiles along the  $c$  axis for both graphite and  $\text{LiC}_6$ . Separate contributions from the  $\sigma$  and  $\pi$  bands are also plotted; a

zero amplitude at  $q = 0$  is expected for the  $\pi$  bands because of their antisymmetric nature. The total profiles are normalized in such a way that integrating from  $-\infty$  to  $\infty$  gives 4 (electrons per carbon atom) in graphite and  $4\frac{1}{6}$  in  $\text{LiC}_6$ . The larger  $\pi$  contribution in  $\text{LiC}_6$  arises from the partly filled antibonding  $\pi$  bands which are almost empty in graphite. For graphite, because the detailed 0.01 eV dispersions along the  $K$ - $H$  direction near the Fermi level are beyond the accuracy of this calculation, the Compton profiles are calculated assuming filled valence bands only.

The Compton profile of graphite was studied by Reed,

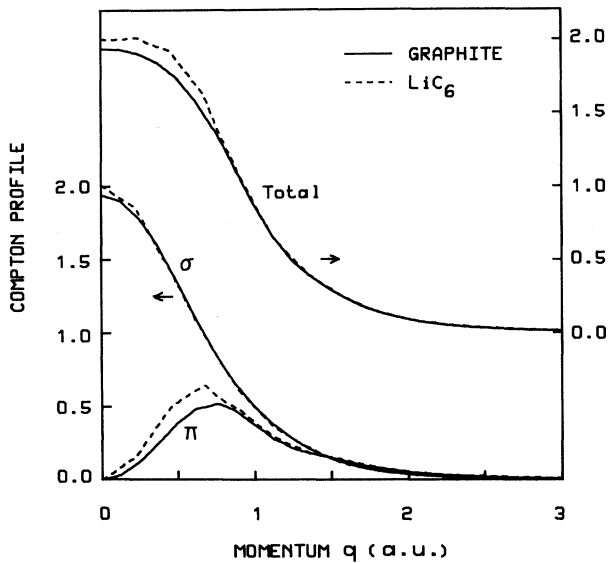


FIG. 1. Comparison of the calculated total Compton profiles of graphite (solid line) and  $\text{LiC}_6$  (dashed line) along the  $c$  axis when appropriately normalized (see text). Separate contributions from  $\sigma$  and  $\pi$  bands and total profiles are shown.

Eisenberger, Pandey, and Snyder<sup>19</sup> using 159 keV  $\gamma$  rays, where directional profiles parallel to the  $c$  axis and averaged over the basal plane were measured. In Fig. 2 we compare the measured values with the theoretical profiles which have been convoluted with the experimental resolution function. The small magnitude of the anisotropy in the profiles (usually less than 3% of the central peak of a valence electron profile) requires that both the theoretical and experimental studies be highly accurate. Although some corrections<sup>20</sup> are expected, they are generally nearly isotropic and do not affect the anisotropy. As is shown in Fig. 2, the agreement between theory and experiment is excellent. Previous calculations of the Compton profiles for graphite had a considerable deviation from the measured anisotropy;<sup>19</sup> the maximum and minimum amplitude of the anisotropic profile differed from the measurements almost by a factor of 2.

To examine the influence of intercalation on the electron momentum distribution, a difference profile is obtained with the graphite profile subtracted from the  $\text{LiC}_6$  profile.

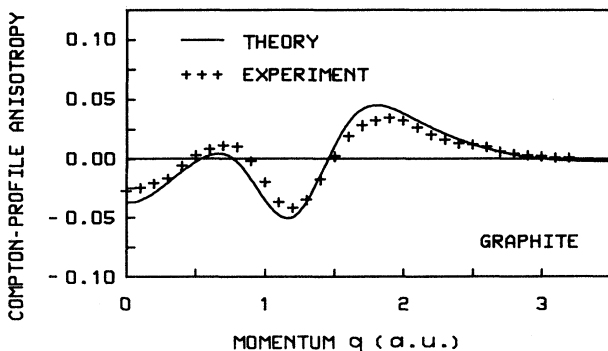


FIG. 2. Comparison of the calculated and experimental anisotropy  $J(\parallel c) - J(\perp c)$  for the Compton profiles of graphite.

The difference curve consists of two parts: one is the contribution from the difference between  $\text{LiC}_6$  and graphite in the profiles of valence bands (filled  $\sigma$  and  $\pi$  bonding states), shown in Fig. 3(a); the other is the contribution from the conduction electrons in  $\text{LiC}_6$  (partly filled  $\pi$  antibonding states), shown in Fig. 3(b). In Fig. 3(a) the difference in the profiles of valence bands is positive for low momenta and negative for high momenta, indicating that the electron charge in  $\text{LiC}_6$  is more spread out into the interlayer region than in graphite. This arises from the lithium potential which causes an intercalant polarization effect tending to pull electrons in the  $\sigma$  and  $\pi$  bonding states toward the lithium atom. In Fig. 3(b), the conduction electron profile in  $\text{LiC}_6$  exhibits some remarkable oscillatory character with valleys near 0,  $G_3$ ,  $2G_3$ , etc., where  $G_3$  (0.90 a.u.) is the shortest reciprocal lattice vector along the  $c$  axis. The physical origin of this effect results from the dispersions along the  $c$  axis, e.g., from  $M$  to  $L$ . According to the self-consistent calculation, states near  $L$  ( $k_z = \frac{1}{2}G_3$ ) are occupied, while states near  $M$  ( $k_z = 0$ ) are not occupied. Contributions from these unoccupied states, which have nonzero coefficients for those plane waves with the  $z$  components of momenta close to integer multiples of  $G_3$ , are excluded from the conduction profile. The fact that  $L$  has lower energy than  $M$  and that the Fermi level lies between them gives rise to valleys appearing at  $nG_3$  ( $n = \text{integer}$ ) in the projected momentum distribution along the  $c$  axis. If  $M$  had lower energy than  $L$  with the Fermi energy in between, the positions of peaks and valleys would be reversed. Hence, this profile in Fig. 3(b) is an indication of the existence of dispersions normal to the basal plane for these conduction bands, which are obtained only when the interlayer interactions are treated properly. The correct magnitude in the difference profile depends on the correctness of the Fermi surface; raising or lowering the Fermi energy can substantially change the shape of the profile. The polariza-

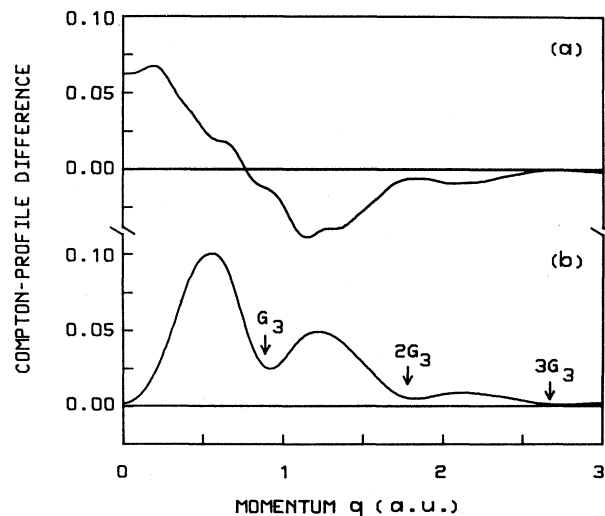


FIG. 3. (a) Difference between the valence-electron profiles and the graphite profiles along the  $c$  axis. (b) The conduction electron contribution from occupied  $\pi$  antibonding states to the Compton profile of  $\text{LiC}_6$  along the  $c$  axis.  $G_3$  (0.90 a.u.) is the shortest reciprocal lattice vector along the  $c$  axis. The curves have been convoluted using a Gaussian function with the full width of half maximum being 0.15 a.u.

tion effect is much weaker here compared to the valence bands<sup>8</sup> due to the symmetry of the antibonding  $\pi$  states, which reduces the interaction between these states and lithium.

The total difference between graphite and  $\text{LiC}_6$  is shown in Fig. 4, which is equal to the sum of profiles in Fig. 3. This is the measurable quantity in experiment and reflects most of the features discussed above. In the rigid-band model, the Fermi level in graphite is raised to accommodate the extra lithium electrons and the Compton profile for these extra states is the difference profile between  $\text{LiC}_6$  and graphite. The large difference between our calculated profile and the rigid-band result is shown in Fig. 4. The rigid-band model predicts a zero amplitude at  $q=0$  (because only extra  $\pi$  antibonding states are filled), and a broader distribution. In contrast, the self-consistent calculation gives a curve containing two features: (1) a nonzero amplitude at  $q=0$  and (2) a narrower distribution with a peak at  $\sim 0.5$  a.u. and dropping to small amplitude at  $\sim 1.0$  a.u. The former comes from Fig. 3(a) and is owing to the intercalant polarization effect for the  $\sigma$  bonding states. The latter corresponds to the first period of the oscillatory curve in Fig. 3(b), which is related to the dispersions along the  $c$  axis with  $L$  below  $M$  and the specific position of the Fermi level. Although other peaks in Fig. 3(b) cannot be seen in Fig. 4, the characteristics of the first period are rather clear. The features discussed above do not appear in the rigid-band model. Hence, although the rigid-band model can describe the qualitative band dispersions of graphite and  $\text{LiC}_6$ , it is not reliable for determining the electron momentum distribution of these materials. Experimental studies of the Compton profiles will provide a critical test of the theoretical predictions made here. Preliminary data<sup>21</sup> in the low- $q$  region favor the calculated results which show a large polarization effect opposite to a rigid-band behavior.

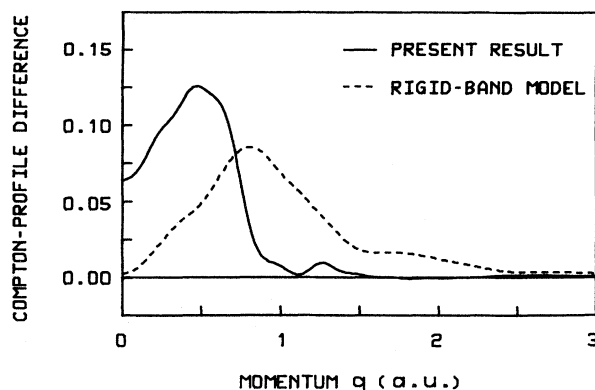


FIG. 4. Difference between the Compton profiles of  $\text{LiC}_6$  and graphite: present self-consistent calculation (solid line) and prediction by the rigid-band model (dashed line). The same convolution function as in Fig. 3 has been used.

We would like to thank Dr. Y. Petroff, Dr. G. Loupiau, and Dr. J. Chomilier for discussions and encouragement, and for sending us the experimental results. This work was supported by National Science Foundation Grant No. DMR7822465 and by the Director, Office of Energy Research, Office of Basic Energy Sciences, Material Sciences Division of the U.S. Department of Energy under Contract No. DE-AC03-76SF00098. One of us (S.G.L.) would also like to acknowledge support by a program development fund from the Director of the Lawrence Berkeley Laboratory. Two of us (M.Y.C. and M.L.C.) wish to acknowledge NATO Research Grant No. RG131.80 which made possible interactions with the Compton scattering experimental groups in Orsay and Paris, France.

<sup>1</sup>J. E. Fischer and T. E. Thompson, *Phys. Today* **31**, 36 (1978).

<sup>2</sup>M. S. Dresselhaus and G. Dresselhaus, *Adv. Phys.* **30**, 139 (1981).

<sup>3</sup>G. K. Wertheim, P.M.Th.M. Van Attekum, and S. Basu, *Solid State Commun.* **33**, 1127 (1980).

<sup>4</sup>W. Eberhardt, I. T. McGovern, E. W. Plummer, and J. E. Fisher, *Phys. Rev. Lett.* **44**, 200 (1980).

<sup>5</sup>E. Cartier, F. Heinrich, P. Pfluger, and H. J. Güntherodt, *Solid State Commun.* **38**, 985 (1981).

<sup>6</sup>Th. Fauster, F. J. Himpsel, J. E. Fischer, and E. W. Plummer, *Phys. Rev. Lett.* **51**, 430 (1983).

<sup>7</sup>N. A. W. Holzwarth, S. G. Louie, and S. Rabii, *Phys. Rev. B* **26**, 5382 (1982).

<sup>8</sup>N. A. W. Holzwarth, S. G. Louie, and S. Rabii, *Phys. Rev. B* **28**, 1013 (1983).

<sup>9</sup>M. L. Cohen and V. Heine, *Solid State Phys.* **24**, 37 (1970).

<sup>10</sup>P. Hohenberg and W. Kohn, *Phys. Rev.* **136**, B864 (1964).

<sup>11</sup>W. Kohn and L. J. Sham, *Phys. Rev.* **140**, A1133 (1965).

<sup>12</sup>L. Hedin and B. I. Lundqvist, *J. Phys. C* **4**, 2064 (1971).

<sup>13</sup>D. R. Hamann, M. Schlüter, and C. Chiang, *Phys. Rev. Lett.* **43**,

1494 (1979).

<sup>14</sup>S. G. Louie, K. M. Ho, and M. L. Cohen, *Phys. Rev. B* **19**, 1774 (1979).

<sup>15</sup>R. C. Tatar and S. Rabii, *Phys. Rev. B* **25**, 4126 (1982), and references therein.

<sup>16</sup>D. Guerard and A. Herold, *Carbon* **13**, 337 (1975); J. Rossat-Mignod, D. Fruchart, M. J. Moran, J. W. Milliken, and J. E. Fischer, *Synth. Met.* **2**, 143 (1980).

<sup>17</sup>P. M. Platzman and N. Tzoar, *Phys. Rev.* **139**, A410 (1965); P. Eisenberger and P. M. Platzman, *Phys. Rev. A* **2**, 415 (1970).

<sup>18</sup>G. Lehmann and M. Taut, *Phys. Status Solidi B* **54**, 469 (1972).

<sup>19</sup>W. A. Reed, P. Eisenberger, K. C. Pandey, and L. C. Snyder, *Phys. Rev. B* **10**, 1507 (1974).

<sup>20</sup>M. Y. Chou, P. K. Lam, and M. L. Cohen, *Phys. Rev. B* **28**, 1696 (1983); G. E. W. Bauer and J. R. Schneider, *Solid State Commun.* **47**, 673 (1983).

<sup>21</sup>G. Loupiau, J. Chomilier, and D. Guerard (private communication).